Case Studies in Thermal Engineering 55 (2024) 104135

Contents lists available at ScienceDirect

Case Studies in Thermal Engineering

journal homepage: www.elsevier.com/locate/csite

Bow-shaped vortex generators in finned-tube heat exchangers; ANN/GA-based hydrothermal/structural optimization

Zhiqing Bai [a], Azher M. Abed [b,j,*], Pradeep Kumar Singh [c,**], Dilsora Abduvalieva [d], Salem Alkhalaf [e], Yasser Elmasry [f], Amani Alruwaili [g], Fawaz S. Alharbi [h], Fahid Riaz [i,***]

[a] School of Intelligent Manufacturing, Anhui Xinhua University, Hefei 230088, Anhui, China
[b] Air Conditioning and Refrigeration Techniques Engineering Department, College of Engineering and Technologies, Al-Mustaqbal University, Babylon, 51001, Iraq
[c] Department of Mechanical Engineering, Institute of Engineering & Technology, GLA University, Mathura, U.P., 281406, India
[d] Tashkent State Pedagogical University, Bunyodkor Avenue, 27, Tashkent, 100070, Uzbekistan
[e] Department of Information Technology, College of Computer, Qassim University, Buraydah, Saudi Arabia
[f] Department of Mathematics - Faculty of Science - King Khalid University, P.O. Box 9004, Abha, 61466, Saudi Arabia
[g] Department of Physics, College of Science, Northern Border University, Arar, Saudi Arabia
[h] Department of Mechanical Engineering, College of Engineering, University of Hafr Al Batin, P.O. Box 1803, Hafr Al Batin, 39524, Saudi Arabia
[i] College of Engineering, Abu Dhabi University, Abu Dhabi, United Arab Emirates
[j] Al - Mustaqbal Center for energy research, Al-Mustaqbal University, Babylon, 51001, Iraq

ARTICLE INFO

Keywords:
Heat transfer improvement
Vortex inducer
Nusselt number
Optimization
Artificial Neural Network
Numerical Model

ABSTRACT

Temperature plays a crucial role in various industries, equipment, and human life, and heat exchangers emerge as fundamental devices in managing this essential parameter. Heat exchangers come in various types, each tailored for specific applications. One commonly utilized variant is the finned-tube heat exchanger, which excels in transferring heat between liquid and gas. This study involved a numerical investigation of a finned-tube heat exchanger equipped with four bow-shaped vortex generators. The primary objective of this study was to assess the influence of three distinct geometric parameters associated with vortex generators on the performance of the heat exchanger. The key performance indicators investigated in this research were the Nusselt number and friction factor, which respectively represent the thermal and hydraulic performance of the device. Also, the relative efficiency index parameter was investigated to evaluate thermal and hydraulic performances simultaneously. Artificial Neural Network and Genetic Algorithm methods were employed to develop response models to simplify and increase the analysis accuracy and determine the optimal geometry. The artificial neural network's prediction models demonstrated high accuracy and effectively forecasted the desired outcomes. It was determined that the relative efficiency index of the finned-tube heat exchanger with vortex generators, even in its weakest-performing design, reached 1.0467. This means that by adding the bow-shaped vortex generators to the heat exchanger, there is a 4.67% increase in the overall performance in the worst case. Also, after predicting the optimal design for the heat exchanger, it was observed that this device has a 13.12% improvement in overall performance compared to the case without

* Corresponding author.
** Corresponding author.
*** Corresponding author.
E-mail addresses: azhermuhson@uomus.edu.iq (A.M. Abed), pradeep.kumar@gla.ac.in (P.K. Singh), fahid.riaz@adu.ac.ae (F. Riaz).

https://doi.org/10.1016/j.csite.2024.104135
Received 18 December 2023; Received in revised form 2 February 2024; Accepted 13 February 2024
Available online 14 February 2024
2214-157X/

vortex generators. To adjust the Nusselt number of the finned-tube heat exchanger lacking vortex generators with that of the finned-tube heat exchanger featuring the optimal design, it is necessary to increase the inlet flow rate of the vortex generators-lacking heat exchanger by 53.20%. This increase in flow rate leads to a significant escalation of 108.73% in the heat exchanger's pumping power compared to the pumping power of the optimal design heat exchanger.

Nomenclature

A_{ht}	heat transfer area (m^2)
B	bias in ANN model
C_p	specific heat capacity (J /kg.K)
D	diameter of tubes (mm)
d_{t1}	transverse distance of 1st column's VGs (mm)
d_{t2}	transverse distance of 2nd column's VGs (mm)
d_l	longitudinal distance of 1st column's VGs (mm)
ff	fraction factor
H	height of fin (mm)
h	heat transfer coefficient $(W/m^2.K)$
k	turbulence kinetic energy (m^2/s^2)
L	length of fin (mm)
L_1	distance of first tube from inlet (mm)
L_2	longitudinal distance of two tubes and two VGs (mm)
m	number of experiments
$\dot{m}$	mass flow rate (g /s)
Nu	Nusselt number
n	number of variables
P	pressure (Pa)
PP	pumping power (mW)
P_k	production of turbulence kinetic energy
Q	transferred heat (W)
Re	Reynolds number
r	radius of VG (degree)
r_{num}	numerical response
r_{pred}	predicted response
S	space between fins (mm)
T	temperature (K)
t	thickness of VG (mm)
V	velocity (m /s)
W	weight in ANN model
w	width of VG (mm)
η	relative efficiency index
ρ	density (kg/m^3)
μ	dynamic viscosity (kg /m.s)
μ_t	turbulence viscosity (kg /m.s)
λ	thermal conductivity (W /m.K)
ω	specific dissipation rate (1 /s)
τ_w	wall shear stress (Pa)

Subscripts

b	base
in	inlet
out	outlet
w	wall

1. Introduction

With the constant advancements in science and technology, the demand for energy continues to rise. However, the limited availability of energy resources and the environmental consequences of excessive energy consumption necessitate the development of efficient plans to maximize the utilization of existing resources [1,2]. Heat exchangers (HEs) are crucial equipment in controlling the temperature of a specific system. They have the ability to adjust the temperature of the target fluid, either increasing or decreasing it based on the system's needs. Also, HEs can use the energy received from a system for other applications to prevent wasted energy [3–6]. Heat exchangers come in various types, each serving different applications [7–9]. One widely used type is the finned-tube heat exchanger (FTHE), which finds extensive usage in diverse sectors such as heating, refrigeration, air conditioning (HVAC&R), chemical industries, and power plants [10,11]. In FTHEs, a series of fins are installed on tube bundles, allowing liquid fluid to flow through the tubes while the gas fluid, which exhibits higher thermal resistance, passes through the spaces between the fins [12]. The thermal performance of heat exchangers can be enhanced through active and passive approaches [13–15]. Among the active techniques, electrodynamics, spray, and vibration of the working fluid or the surface in contact with the fluid can be mentioned, which are done to intensify the heat exchange in the device [16]. On the other hand, passive methods involve modifying the geometry of the heat exchangers to improve performance [17–19]. In the case of FTHEs, altering the gas side geometry disrupts the growth of boundary layers, thereby reducing thermal resistance and enhancing thermal performance [12,20]. Recent years have witnessed a proliferation of research efforts aimed at enhancing the performance of heat exchangers, with particular emphasis on passive methods [21–24], particularly in the context of FTHEs. One of the ways to increase heat transfer passively in FTHE is to add vortex generators (VGs) to heat exchangers [25]. VGs are designed to induce controlled swirling motion or vortices in the fluid flow. When the fluid encounters the surface of the VGs, it undergoes local acceleration and deceleration, resulting in the formation of vortices. These vortices can enhance mixing and promote better heat transfer by disrupting the boundary layer and bringing fresh fluid into contact with the heat exchange surfaces. In addition, vortex generators can be designed to direct the fluid flow in the desired direction so that in a particular place, they cause the fluid to mix and collide with the thermal walls to increase the heat transfer. It should also be noted that adding VGs will increase the heat transfer area to some extent. Therefore, choosing the shape, size, and location of these parts in heat exchangers is very important and influential [26]. Dogan and Erzincan [27] analyzed the effect of the transverse and longitudinal pitch ratios between novel vortex generators experimentally. Their observation noted that the decrease in transverse and longitudinal pitch ratios increased both the *Nu* and *ff*. Researchers found that the highest level of thermal improvement was attained when the VGs configuration was inline, and the value of transverse pitch ratio and longitudinal pitch ratio parameters were equal to 0.16 and 1.5, respectively. Sadeghianjahromi et al. [28] conducted a comprehensive numerical investigation on a three-dimensional FTHE featuring wavy fins. Their study focused on enhancing the heat exchanger's performance by incorporating louvers and VGs on the fins. According to their findings, adding louvers led to a remarkable reduction of 16% in thermal resistance, while implementing VGs decreased thermal resistance by 18%. Fiebig et al. [29] studied the impact of vortices generated by VGs attached to fins on heat transfer performance. The study findings indicate that delta wings exhibit greater effectiveness than rectangular wings in enhancing heat transfer. Wang et al. [30] used a computational fluid dynamic (CFD) simulation to determine the effect of three geometric characteristics, including fin spacing, ellipticity tube diameter ratio, and ellipticity tube inclination, on heat exchanger performance in various Reynolds numbers. They found that the best thermo-hydraulic efficiency was achieved in the FTHE with a tube diameter ratio of 0.6 and a tube inclination of 30°. Naik and Tiwari [12] conducted a study on the impact of utilizing rectangular winglet pairs on the performance of FTHE. Their investigation led to the conclusion that selecting the optimal locations for the winglets could considerably enhance the thermal performance of the heat exchanger. Kumar et al. [31] researched the optimization of the absorber plate with delta-shaped winglets for solar air heaters. They observed that the delta-shaped winglets improved *Nu* by 5.17 times and *ff* by 4.52 times. Lotfi et al. [32] used three different VGs to run CFD simulations to test the performance of FTHE. They found that the heat exchanger's overall performance has a direct relationship with the height of the wavy fins and an inverse relationship with the value of the diameter ratio of the ellipticity tube. Tian et al. [33] tested the effect of different winglets and concluded that the delta-shaped winglets show worse thermal performance than the rectangular winglets. Kaood et al. [34] investigated the thermal-hydraulic characteristics of turbulent water flow within distinct conical tubes with varying diameter ratios. The study scrutinizes tubes with and without dimpled surfaces, comparing them with the thermal-hydraulic characteristics of conventional straight-smooth tubes. The research revealed that the convergent tube featuring dimples (with a diameter ratio of 1.5) demonstrated the highest overall performance value, exhibiting a 29.54% improvement compared to the smooth tube geometry with a diameter ratio of 1. Demirag et al. [35] researched heat transfer enhancement using a novel type of conic vortex generator. This work used experimental and numerical methods to analyze the effect of VG's attack angle, blade angle, and scale ratio on thermal performance. According to the experimental results, the authors reported that the highest thermal performance is obtained at attack angle = 37.5°, blade angle = 30°, and scale ratio = 1:1. In a study conducted by Torii et al. [36], the impact of wing placement and size on the thermohydraulic behavior of FTHE was examined through experimental means. The findings revealed that in an in-line tube configuration, the pressure drop decreased by 8–15%, while the heat transfer increased by 10–20%. Additionally, for a staggered tube arrangement, the pressure drop experienced a 34–55% reduction, accompanied by an improvement in heat transfer by 10–30%. Kaood and Fadodun [37] investigate turbulent entropy production rates in convergent and divergent pipes with and without twisted tape inserts. Results indicate that twisted tape inserts increase viscous entropy production rates while reducing thermal entropy production rates. Additionally, thermal entropy production rates are higher in divergent pipes, while viscous entropy production rates are higher in convergent pipes. New correlations using response surface methodology were developed to estimate entropy production rates, with Reynolds number and diameter ratio proving statistically significant.

By employing suitable testing equipment and methods, experimental studies have the potential to yield more precise and realistic outcomes. However, conducting such research can be expensive, time-consuming, and reliant on specialized equipment that may not always be readily available. To mitigate these challenges, researchers have turned to numerical methods such as finite element and finite volume methods, which have helped reduce the costs and time associated with experiments. Nevertheless, numerical methods also come with their own drawbacks, including high computational and equipment expenses. To address these issues, researchers have embraced prediction methods like artificial neural network (ANN), which functions as a black-box regression model. This computationally efficient model is a viable alternative to resource-intensive numerical models, allowing for the prediction of test results and alleviating associated challenges [38,39]. Recent advancements in machine learning have led to the emergence of new computational approaches, particularly artificial neural networks (ANN), which have captured the attention of numerous researchers in predicting the outputs of complex systems. Additionally, these methods have been widely utilized in various studies involving different types of heat exchangers [40]. On the other hand, various methods are used to optimize the obtained model parameters and results. Genetic algorithm (GA) is a stochastic calculation method inspired by Darwin's principle of evolution and solves optimization problems well [41]. Li et al. [42] modeled a disk-shaped microchannel heat sink using numerical simulations and ANN and RSM methods. They selected three geometrical parameters, including the microchannel's growth angle and the circular fin's diameter and height, as the input variables of the investigation. Their research states that increasing all three parameters increases the heat transfer of the device. In their scholarly article, Mohammadi et al. [43] conducted a numerical experiment on a shell-and-tube heat exchanger comprising six porous baffles. The primary objective of their investigation was to analyze the characteristics of heat transfer rate and pressure drop in the heat exchanger. To optimize the thermo-hydraulic performance of the system, the researchers employed ANN and GA methods. According to their findings, it was determined that the heat exchanger with a baffle cut of 25.68%, a permeability of $10{-}9\ m^2$, and a porosity of 21.68% represents the most optimal design, resulting in reduced pressure drop and enhanced heat transfer rate. The performance of a double-tube heat exchanger equipped with twisted strip inserts and working fluid of water-Fe_2O_3 nanofluid was studied using ANN under the Levenberg-Marquardt (LM) learning algorithm by Aghayari et al. [44]. The results obtained from their research showed that using a concentration of 0.1% by volume of Fe_2O_3 particles in water increases *Nu* by 25% and *ff* by 6.3%. Sharifi et al. [45] used ANN and GA to predict the most suitable design of spiral wire inserted in the tube to optimize the hydraulic and thermal performance of the heat exchanger. They found that a suitable spiral wire generally increases heat transfer efficiency, but the wrong wire selection may unexpectedly decrease the device's efficiency. Chamoli [46] studied the influence of V-shaped perforated baffles on the rectangular channel's heat transfer and friction factor using response surface methodology (RSM) and ANN methods. The author calculated the most optimal results in the fluid flow with a Reynolds number of 18500 and geometrical specifications as roughness to height ratio of 0.33, baffle pitch to roughness ratio of 2.6, and open area ratio of 18%. Xie et al. [47] optimized FTHE by using rectangular vortex generators. In this optimization, they utilized ANN and RSM methods and presented a new FTHE design with an improvement of 25.5% compared to the primary heat exchanger. Using ANN, Rahman and Zhang [31] predicted the thermoacoustic heat exchanger's heat transfer coefficient. They investigated the oscillation frequency and average pressure, which are two variables affecting heat transfer. Xie et al. [48] presented models to estimate *Nu* and *ff* of an FTHE with triangular VGs using a multi-layer artificial neural network. They stated that the deviation between the data predicted by the models obtained by ANN and the experimental data is less than 4%, indicating the models' high accuracy.

FTHEs are among the most widely used heat exchangers in various industries and people's daily lives. Therefore, optimizing the performance of these devices is an essential thing that can have many advantages. By optimizing FTHEs, it is possible to bring achievements such as increasing performance, saving cost and energy, reducing environmental effects, and innovation and technological progress. Increasing the efficiency of heat exchangers can be achieved through a range of active and passive techniques, with one of the most prevalent and cost-effective methods being the utilization of vortex generators. This method tries to increase the heat transfer coefficient on the gas side that passes between the fins by creating vortices and continuously breaking the thermal boundary layer. The main goal of this study is to optimize the thermal-hydraulic performance of an FTHE by adding four bow-shaped VGs on the fins. A hybrid computational approach combining CFD and ANN was employed to achieve this. One of the reasons for using this type of VG is to direct the fluid flow from the outside of the channels to the inside and around the tubes. On the other hand, these VGs can create larger and more vortices behind them. Also, this shape can generate less drag, improving the flow's hydraulic performance compared to other shapes. Three geometric parameters of the VGs (d_{t1}, d_{t2}, and d_l) were considered as input variables, while the

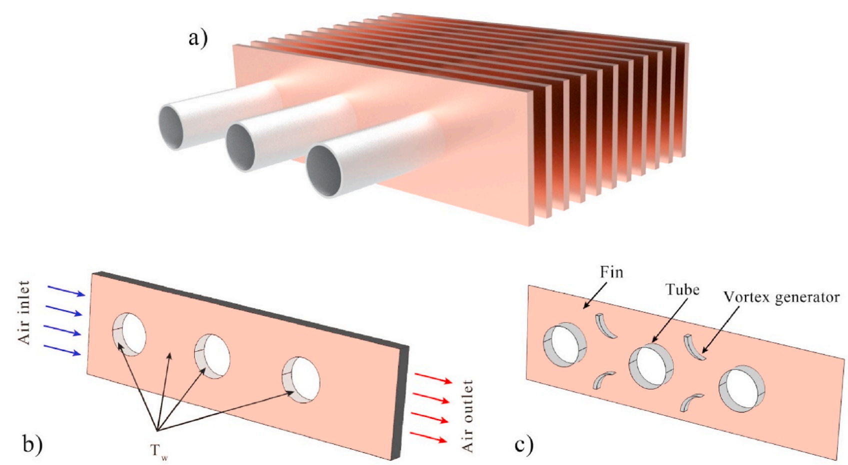

Fig. 1. (a) The design of the basic FTHE, (b) the simulated geometry, (c) view of the between two fins.

parameters *Nu* and *ff* served as the research responses. Through changing these geometric parameters, the configuration of VGs on the fins is altered, thus influencing fluid flow dynamics. Based on the numerical analysis results, separate ANNs were trained for each response, and prediction models were developed for each. These models effectively forecast thermal-hydraulic performance using designated inputs without requiring high expenses, intricate computations, and extended durations. This approach is highly beneficial for designing and constructing finned-tube heat exchangers. Ultimately, single-objective and multi-objective optimizations were done, and the optimal designs of FTHE for different conditions were predicted using prediction models and GA.

2. Methodology

2.1. Physical structure of FTHE

As mentioned in the previous section, an FTHE according to the reference model [49] was presented and investigated in this research. As depicted in Fig. 1, the investigated heat exchanger consists of three circular tubes arranged in series along the central line of the fins. Rectangular fins are utilized in this FTHE design, and four VGs are installed on one side of these fins. In this study, an attempt was made to increase the heat absorption capacity of the air by augmenting the heat transfer coefficient on the air side. A single gap between two fins was selected for the numerical simulation according to symmetry in the geometry and boundary conditions. Fig. 2 showcases the simulated FTHE geometry, along with the arrangement of the VGs and relevant structural parameters. The values of the mentioned parameters are presented in Table 1. Within this table, H and L denote the height and length of the fins, respectively. D represents the diameter of the identical tubes, while L_1 signifies the distance of the first tube from the inlet, and L_2 represents the longitudinal distance between the two tubes and two VGs. In a vortex generator, t, w, and r show the VG's thickness, height, and radius, respectively. Additionally, d_{t1} and d_{t2} denote the distances of the first and second pairs of vortex generators from the sides, respectively. Lastly, d_l represents the distance between the VG and the air inlet.

2.2. Mathematical formulations and boundary conditions

The CFD method was used to investigate the selected geometry numerically, and this analysis was done using COMSOL Multiphysics software. This software utilizes the finite element method (FEM) to solve the numerical analysis, which is a widely used approach for solving differential equations derived from engineering and mathematical modeling. This study determined the boundary conditions and assumptions based on the specific geometry and fluid flow conditions to overcome computational complexities.

- A steady and turbulent flow regime was considered in the modeling process, and the Re is constant and equal to 500 ($\dot{m} = 0.1169$ g/s).
- The fluid used in the simulation is air, and it was considered incompressible, Newtonian, and viscous.
- The constant thermophysical characteristics of air are illustrated in Table 2.
- The conditions of no-slip velocity and no-temperature jump on the walls in contact with the air were considered.
- Thermal radiation and heat dissipation were neglected.
- The wall temperature (T_w) in contact with air (tubes, fins, and the vortex generators) was considered 330 K.
- The air inlet temperature (T_{in}) was assumed to be 300 K.

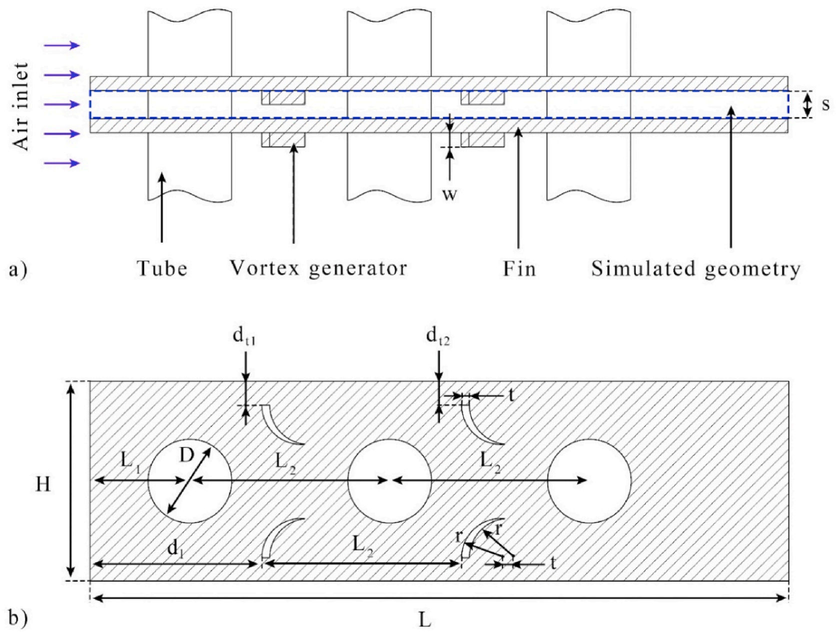

Fig. 2. (a) Top view of simulated geometry, (b) geometric specifications of the FTHE and VGs.

Table 1
Dimensional parameters of geometry used in numerical simulation.

Geometric specifications	Value (mm)
D	10.656
L	88.92
L_1	12.708
L_2	25.416
H	25.416
r	5
S	3.6
t	1
w	1.8

Table 2
Thermophysical characteristics of air at a temperature of 300 K [50].

Property	Value
ρ (kg/m^3)	1.177
C_p (J/kg.K)	1006
λ (W/m.K)	0.0262
μ (kg/m.s)	1.84x10^{-5}

Table 3
Constant parameters pertaining to the SST k-ω turbulence model.

Constant	Value
a_1	0.31
β^*	0.09
β_1	0.075
β_2	0.0828
γ_1	0.5532
γ_2	0.4404
σ_{k1}	0.85
σ_{k2}	1.0
$\sigma_{\omega 1}$	0.5
$\sigma_{\omega 2}$	0.856

- The pressure at the air outlet was considered 0 Pa.

The simulation's governing equations consist of continuity, momentum, and energy equations, which are correspondingly represented by Eqs. (1)–(3) [49].

$$\nabla.\left(\rho\vec{V}\right) = 0 \tag{1}$$

$$\vec{V}.\nabla\left(\rho\vec{V}\right) = -\nabla P + \nabla.\left[(\mu+\mu_t)\left(\nabla\vec{V} + \left(\nabla\vec{V}\right)^T\right)\right] \tag{2}$$

$$\vec{V}.\nabla(\rho C_p T) = \nabla.\left[\left(\lambda + \frac{\mu_t}{Pr}\right)\nabla T\right] \tag{3}$$

where V, P, T, C_p, and λ are the fluid's velocity, pressure, temperature, specific heat capacity, and thermal conductivity, respectively. Additionally, the parameters μ, μ_t, and Pr correspond to the fluid's dynamic viscosity, turbulence viscosity, and Prandtl number, respectively. The Shear Stress Transport (SST) turbulence model was chosen because of its enhanced ability to predict internal flow behavior accurately and flow involving discrete regions. This model uses the well-established and accurate k–ω model, initially devised by Wilcox [51,52], to capture turbulence characteristics near the wall. Simultaneously, it employs the conventional k–ε model, which is suitable for regions away from the wall, by utilizing a blending function. By adopting the SST model, the transport equations for turbulence kinetic energy (k) and specific dissipation rate (ω) are formulated as described in Ref. [53]:

$$\rho\vec{V}.\nabla k = \nabla.[(\mu+\mu_t\sigma_k)\nabla k] + P - \beta^*\rho k\omega \tag{4}$$

$$\rho\vec{V}.\nabla\omega = \nabla.[(\mu+\mu_t\sigma_\omega)\nabla\omega] + \frac{\gamma}{\mu_t}\rho P - \rho\beta\omega^2 + 2(1-F_1)\frac{\rho\sigma_{\omega 2}}{\omega}.\nabla\omega.\nabla k \tag{5}$$

$$\mu_t = \rho \frac{a_1 k}{\max(a_1 \omega, SF_2)} \tag{6}$$

$$S = \sqrt{2S_{ij}S_{ij}} \tag{7}$$

$$P = \min(P_k, 10\rho\beta^* \omega k) \tag{8}$$

$$p_k = \mu_t \left[\nabla\vec{V} : \left(\nabla\vec{V} + \left(\nabla\vec{V}\right)^T\right)\right] \tag{9}$$

$$F_1 = \tanh\left[\left(\min\left(\max\left(\frac{\sqrt{k}}{\beta^* \omega y}, \frac{500\mu}{\rho\omega y^2}\right), \frac{4\rho\sigma_{\omega 2} k}{\left(\max\left(\frac{2\rho\sigma_{\omega 2}}{\omega}.\nabla k.\nabla\omega, 10^{-20}\right)\right)y^2}\right)\right)^4\right] \tag{10}$$

$$F_2 = \tanh\left[\left(\max\left(\frac{2\sqrt{k}}{\beta^* \omega y}, \frac{500\mu}{\rho\omega y^2}\right)\right)^2\right] \tag{11}$$

$$\beta = F_1\beta_1 + (1 - F_1)\beta_2 \tag{12}$$

$$\gamma = F_1\gamma_1 + (1 - F_1)\gamma_2 \tag{13}$$

$$\sigma_k = F_1\sigma_{k1} + (1 - F_1)\sigma_{k2} \tag{14}$$

$$\sigma_\omega = F_1\sigma_{\omega 1} + (1 - F_1)\sigma_{\omega 2} \tag{15}$$

Within the equations above, P_k denotes the production of k resulting from the mean velocity gradients. F_1 and F_2 represent the blending functions and vary in the range of 0–1. The subsequent equations were employed to assess the thermal-hydraulic efficiency of the FTHE equipped with bow-shaped VGs [10,54].

$$Re = \frac{\rho V.2S}{\mu} \tag{16}$$

$$LMTD = \frac{\Delta T_h - \Delta T_c}{\ln\left(\frac{\Delta T_h}{\Delta T_c}\right)} = \frac{(T_w - T_{out}) - (T_w - T_{in})}{\ln\left(\frac{T_w - T_{out}}{T_w - T_{in}}\right)} \tag{17}$$

$$Q = \dot{m}C_p(T_{out} - T_{in}) \tag{18}$$

$$h = \frac{Q}{A_{ht}.LMTD} \tag{19}$$

The Nusselt number, a dimensionless quantity named after Wilhelm Nusselt, is a fundamental parameter in convective heat transfer analysis. It characterizes the efficiency of heat transfer between a solid surface and a fluid in motion. Defined as the ratio of convective to conductive heat transfer within a fluid boundary layer, the *Nu* holds paramount significance in understanding and quantifying heat exchange phenomena. In essence, it encapsulates the influence of fluid flow behavior on heat transfer rates, serving as a crucial metric in the design and optimization of various engineering systems such as heat exchangers, cooling systems, and aerodynamic profiles. The Nusselt number's capability to unify complex heat transfer processes into a single, interpretable value underscores its pivotal role in advancing thermal science and engineering applications. The general form of the equation of this parameter is presented in Eq. (20) [10,49]. The friction factor, an essential parameter in heat exchanger design and analysis, characterizes the resistance encountered by a fluid as it flows through a conduit. The *ff* assumes paramount importance in heat exchangers, where efficient fluid flow is imperative for optimal heat transfer. It quantifies the energy loss due to viscous effects within the fluid boundary layer, influencing the *ΔP* across the heat exchanger and subsequently affecting overall system performance. Accurate determination of the *ff* aids in assessing the pumping power required to maintain desired flow rates, thereby enabling engineers to strike a delicate balance between efficient heat transfer and operational energy expenditure. Consequently, a comprehensive understanding of the *ff* is indispensable for achieving the desired thermal performance while ensuring the economic viability of heat exchanger operations. The calculation method of this parameter is reported in Eq. (21) [49].

$$Nu = \frac{h.2S}{k} \tag{20}$$

$$ff = \frac{\Delta P}{\frac{1}{2}\rho V^2}\frac{2S}{L} \tag{21}$$

$$PP = \frac{\dot{m}}{\rho}\Delta P \tag{22}$$

In the above equations, parameter *2S* is the channel's characteristic dimension between two fins, which is used instead of the hydraulic diameter in these heat exchangers [10,49], and *L* indicates the length of channels and fins. *Nu*, *h*, *Q*, and *ff* are Nusselt number, heat transfer coefficient, heat absorbed by air, and friction factor, respectively. In the following, to have a general criterion for simultaneously checking the heat exchanger's thermo-hydraulic performance, the relative efficiency index was presented according to Eq. (23) [55,56], which shows the improvement of the overall performance of the presented FTHE compared to the basic design of the heat exchanger, which is the design without VGs. Here, the parameters with a subscript of *b* are the data for the heat exchanger without vortex generators.

$$\eta = \frac{Nu/Nu_b}{(ff/ff_b)^{1/3}} \tag{23}$$

2.3. Validation of numerical method and mesh independence test

To guarantee the precision and reliability of the numerical simulation outcomes, a comparison was made between the thermal-hydraulic parameters obtained by the numerical method of the present work and the experimental work of Wang et al. [57], which pertained to an FTHE configuration featuring four rows of tubes (Fig. 3a and b). Additionally, the numerical method data were compared with the numerical study results of Sinha et al. [49], as shown in Fig. 3c and d. Also, the configurations examined in the

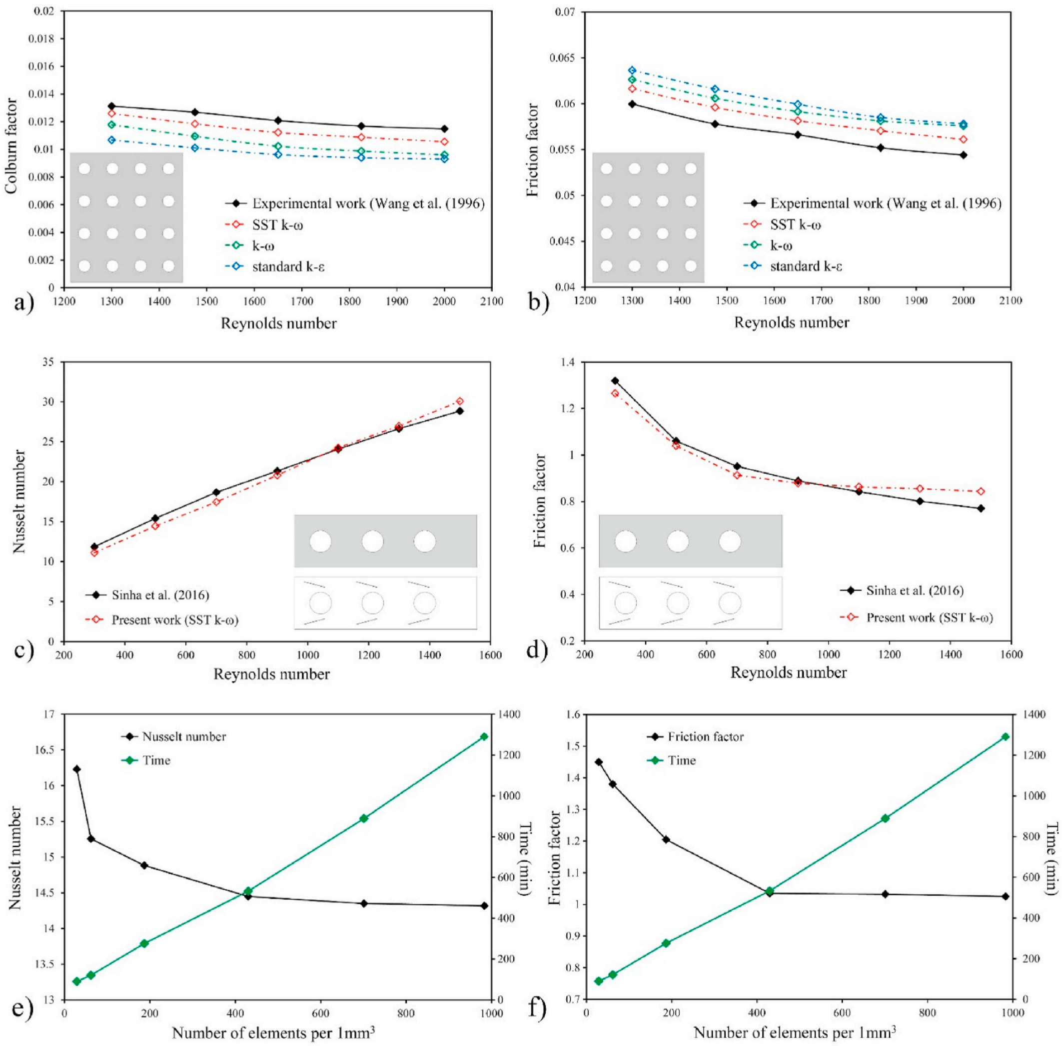

Fig. 3. Validation of the (a) thermal and (b) hydraulic results of the current research with experimental work of Wang et al. [57]. Validation of the (c) thermal and (d) hydraulic results of the current research with a numerical study of Sinha et al. [49]. Mesh independence test in conditions of Re = 500, T_{in} = 300 K, and T_w = 330 K for (e) thermal and (f) hydraulic performances.

reference studies were presented in the corresponding plots. The reason for the validation of a numerical work in addition to the experimental work is to strengthen the validity of the numerical analysis of the present work and also to show the agreement of the results with the numerical results. Because the possibility of error occurring in both experimental and numerical studies is somehow possible. Therefore, validating the results of the used numerical method with both experimental and numerical results, it guarantees that the used numerical method is valid. It should also be noted that the present work's FTHE configuration inspired the heat exchanger configuration of Sinha et al. [49]. Considering that this heat exchanger does not have many tubes, the effect of vortex generators in this design will be significant and more visible. The results obtained from these comparisons demonstrated a suitable accordance between the thermal-hydraulic outcomes of the numerical simulations and the findings reported in the referenced studies. Consequently, the validity of the numerical analysis for the selected geometry and physics was confirmed, allowing it to be used for the rest of the research. Table 4 presents the deviations between the experimental measurements and the results obtained by the numerical method of the present work. These differences could be attributed to various factors, including measurement errors, model assumptions, and simplifications inherent in the numerical simulations. Also, the average deviation, which measures the overall agreement between the experimental and numerical data sets, was presented in this table.

In order to choose the appropriate turbulence model, three models, SST k-ω, k-ω, and standard k-ε were used in the numerical simulation of the geometry presented by Wang et al. [57] and compared with the results reported in that work. As can be seen, the outcomes derived from implementing the SST k-ω turbulence model exhibit a higher level of concurrence with the findings of the experimental study. Also, the value of $y+$ calculated using Eq. (24) equals the average value of 1.86. For $y+$ values lower than 30 and especially close to 1, using the Low Reynolds Number (LRN) wall model in the simulations is suggested to predict the fluid behavior near the walls. This wall model finds application in the SST k-ω and k-ω turbulence models, indicating the general unsuitability of the k-ε method for this research. In Eq. (24), the parameters τ_w and y express the wall shear stress and the distance from the wall to the center of the element in contact with the wall, respectively [58].

Discretizing the geometry into smaller sizes is essential for conducting numerical analysis using the finite element method. The selection of an appropriate meshing is crucial to ensure that the thermal-hydraulic results are independent of the number of mesh elements. The simulation domain meshing in this study was accomplished using the COMSOL Multiphysics software. The independence of the present study's results from the mesh element number was verified and documented in Fig. 3e and f. According to the results in different mesh element sizes, it is seen that the simulation with 433 elements per 1 mm^3 is optimal, and the results do not change much by making the meshes smaller. The free tetrahedral mesh type, depicted in Fig. 4, was employed in this study. Also, a convergence criterion of 10^{-6} was set for each physics component utilized in numerical simulation.

$$y+=\frac{\rho y\sqrt{(\tau_w/\rho)}}{\mu} \tag{24}$$

2.4. Implementation of ANN method and multi-objective optimization

As mentioned earlier, one of the ways to reduce the problems of utilizing experimental and numerical methods, each of which has different problems, is to use data-driven black-box models. These models aim to establish relationships between input data and desired responses, regardless of the possible physical connections between parameters. ANNs have gained significant popularity across various fields [59], drawing inspiration from the information processing capabilities of the biological nervous system [60]. Due to the potential of ANN to solve ill-defined or nonlinear problems in engineering, business, health, etc., it has become increasingly popular among researchers in recent years [61]. Fig. 5a is related to the architecture schematic of the ANN used in this study, which consists of three separate layers named input, hidden, and output. The computational performance of the neurons in the hidden and output layers is shown in Fig. 5b. For the acquisition of individual models for each response in the mentioned approach, MATLAB (2016b) software was employed, utilizing the Levenberg-Marquardt (LM) method for training purposes. A data split of 70% for training, 15% for validation during training, and 15% for post-training model testing were performed. The random selection of these data was implemented to avoid any learning bias. The activation function chosen for the hidden layer neurons was the tangent-sigmoid, in alignment with the network requirements. Furthermore, the output layer neuron utilized a linear activation function, signifying that its output equates to the value of the corresponding response parameter. Of course, it should be noted that the input and output parameters of the ANN were used in normalized form. Finally, three parameters of determination coefficient (R^2), normalized standard deviation (Δq), and root mean square error (RMSE) were used to compare the results of the numerical simulation and the results of the ANN's models

Table 4
Deviations between experimental and numerical data.

Data point	Deviation between Wang et al. [57] validation data		Deviation between Sinha et al. [49] validation data	
	Colburn factor	Friction factor	Nusselt number	Friction factor
1	0.5249×10^{-3}	0.1674×10^{-2}	0.7429	0.0544
2	0.8345×10^{-3}	0.1809×10^{-2}	0.9703	0.0211
3	0.8628×10^{-3}	0.1540×10^{-2}	1.2100	0.0379
4	0.8086×10^{-3}	0.1851×10^{-2}	0.5355	0.0101
5	0.9275×10^{-3}	0.1709×10^{-2}	0.1892	0.0208
6	–	–	0.3387	0.0536
7	–	–	1.2373	0.0731
Average	0.7917×10^{-3}	0.1717×10^{-2}	0.7463	0.0387

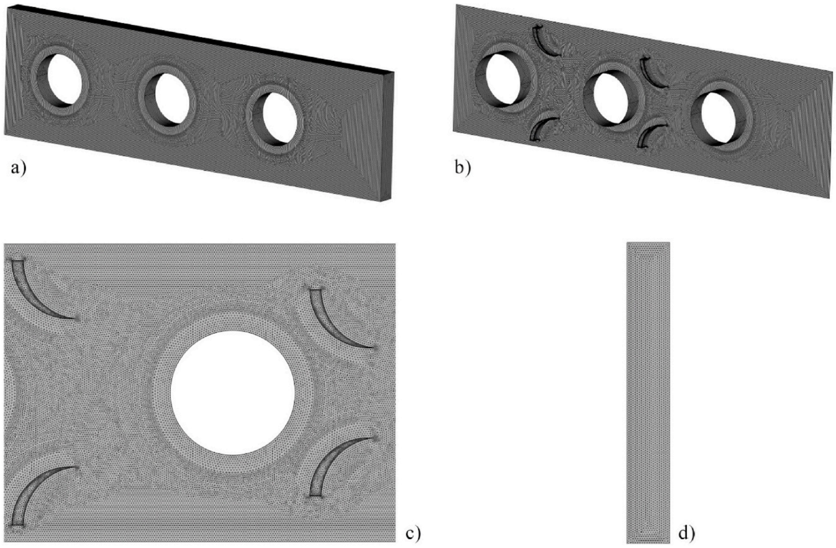

Fig. 4. Mesh created on simulated geometry from different views.

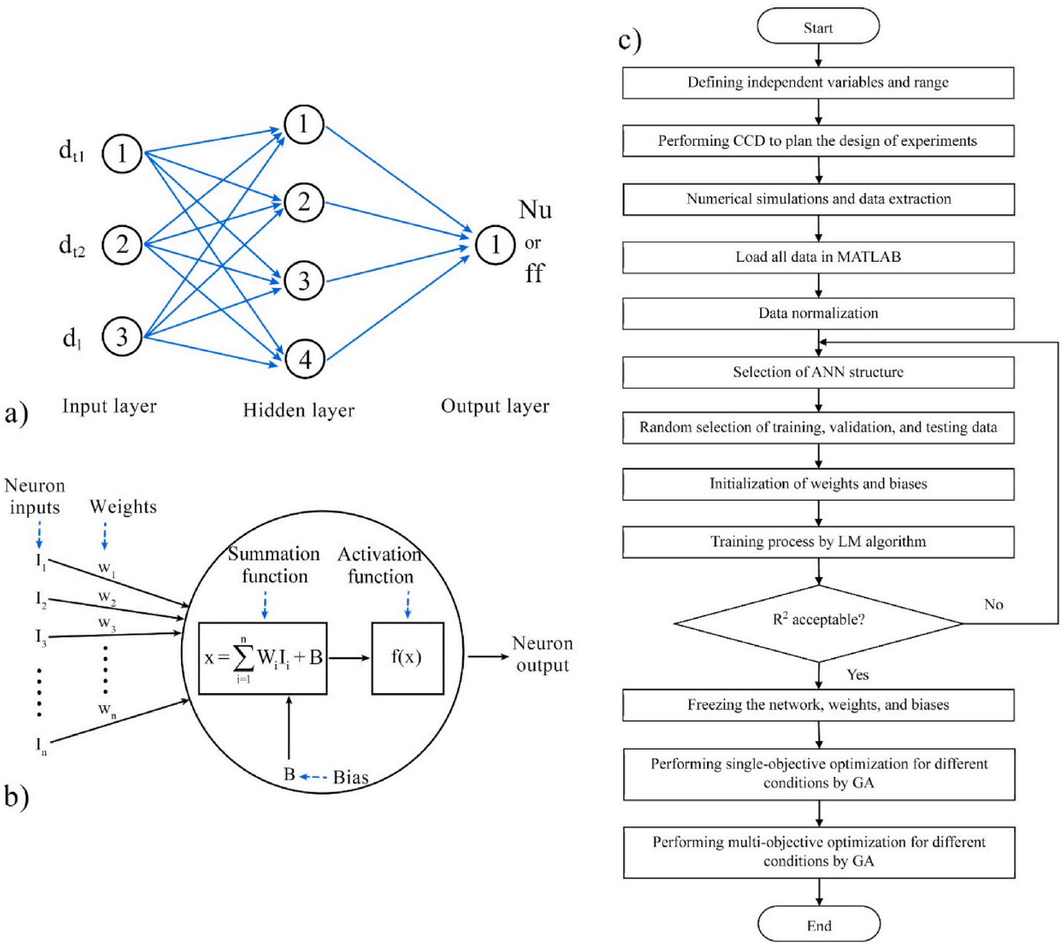

Fig. 5. (a) The 3-4-1 artificial neural network architecture was used for each response individually, (b) the function of neurons in the hidden and output layers, (c) the flow chart of research.

[62]. Fig. 5c shows the flow chart of the present work. This flow chart delineates the intricate web of activities undertaken during the current research, offering a visual roadmap to the various vital elements that constitute the foundation of this work.

Three geometric parameters were selected for modeling and optimization, which are presented in Table 5, along with the range of changes. The central composite design (CCD) method [63] and these parameters were utilized to provide 15 different geometries for numerical simulation and extraction of thermo-hydraulic results. These 15 geometric combinations are also shown in Table 6. The CCD method was implemented to optimize efficiency and conserve valuable time and energy resources by minimizing the requirement for extensive testing procedures.

The resolution of most engineering predicaments necessitates the employment of optimization methodologies, either in a parametric or mathematical context. When a predictive model underpins the approach, mathematical optimization methodologies emerge as the favored choice due to their capability to explore design points spanning the design space. The pursuit of refining a specific engineering predicament's performance and its subsequent optimization in terms of various established parameters has driven numerous researchers to devise a spectrum of performance metrics. It is worth noting that solitary optimization methods often grapple with accuracy concerns, primarily attributed to their tendency to yield a sole optimized design point within the entire solution space. In contrast, the domain of multi-objective optimization engenders a collection of Pareto-optimal solutions, wherein objective functions are either minimized or maximized while adhering to prescribed design constraints. Among the panoply of optimization methodologies introduced, the Genetic Algorithm (GA) emerges as a recent and pertinent approach, distinguished by its adeptness in optimizing intricate non-differentiable, implicit, and multi-objective challenges, outshining alternative techniques in this capacity. In the present work, both single and multiple optimization types were used, and the results of both modes have been reported and reviewed. In all tests related to optimization using GA, population, and generation were considered 1000 and 300, respectively.

3. Results and analysis

3.1. Findings of the numerical approach

Table 7 exhibits the outcomes derived from numerical simulation methods and ANN models for the *Nu* and *ff* responses. Analyzing the data reveals that the highest *Nu* value is obtained in the 7th test, indicating superior heat transfer in this particular geometry. Conversely, the lowest *Nu* value and heat transfer correspond to the 15th test. In Fig. 6a, the temperature at the outlet of the 7th test is more uniform and higher than in the 15th test because the temperature in the lower and upper part of the 15th geometry is lower and has a lower temperature on average. The lower air temperature at the outlet means that the heat absorption from the walls by air is weak, and heat transfer is not done well. The reason for this issue can be understood according to Fig. 7. In the 7th test, the placement of VGs significantly increases the formation of vortices while restricting the airflow from the sides and directing it toward the center of the track. On the contrary, in the 15th experiment, the airflow bypasses the VGs and tubes and passes through the sides of the path, which reduces the collision of thermal surfaces and also the generation of vortices. In the following, the hydraulic performance on the air side of FTHE was examined, and it was observed that the lowest and highest *ff* belong to the 15th and 9th experiments, respectively. The *ff* has a direct relationship with the pressure drop, and this issue can also be seen in Fig. 6b. In the 9th test, the vortex generators blocked the airflow and prevented the flow from passing easily, and this subject increased the pressure drop. Still, in the 15th test, as mentioned above, the sides of the way are free, the flow passes quickly, and less pressure drop occurs. Also, according to the data related to η in Tables 7 and it can be seen that, in general, adding these VGs increases the overall performance of the heat exchanger because the value of this parameter is above 1 for all designs. In the following, the analysis of ANN models was carried out to investigate more precisely the effect of placement of VGs on FTHE performance.

3.2. Findings of the ANN method

Two separate artificial neural networks with the same architecture for each response (*Nu* and *ff*) were trained and tested to derive a particular model for each response. The ANNs consist of three layers, and there are three neurons equal to the inputs in the first layer. The second layer (hidden layer) contains four neurons, and in the third layer (output layer), there is one neuron. Based on the selected network structure, there are 21 parameters, including weights and biases in each network, which were optimized by the Levenberg-Marquardt method and training and testing. These parameters for the *Nu* and *ff* models are shown in Eqs. (25)–(28). The final model provided by ANN for *Nu* is given in Eq. (26). The precision of this model in predicting the response according to the R^2 parameter presented in Table 8 is 99.88%. That is, this equation cannot correctly predict only 0.12% of the data, which is negligible.

Table 5
Selected input parameters and levels to extract models and perform optimization.

Input variables	Levels of variable		
	−1	0	+1
d_{t1} (mm)	1	3	5
d_{t2} (mm)	1	3	5
d_l (mm)	18	21.5	25

Table 6
Selected values of variables for numerical testing.

Test	Variables		
	d_{t1} (mm)	d_{t2} (mm)	d_l (mm)
1	3	5	21.5
2	5	3	21.5
3	3	3	21.5
4	5	5	18
5	3	3	25
6	5	1	18
7	3	1	21.5
8	3	3	18
9	1	1	18
10	1	5	25
11	1	1	25
12	1	3	21.5
13	1	5	18
14	5	1	25
15	5	5	25

Table 7
Comparison of responses predicted by ANN models and obtained by the numerical method for experiments.

Run	*Nu*		*ff*		*η*	
	Numerical	ANN	Numerical	ANN	Numerical	ANN
1	13.5034	13.5032	0.9128	0.9128	1.0935	1.0934
2	13.1683	13.1717	0.8848	0.8848	1.0774	1.0777
3	13.6611	13.6646	0.9468	0.9468	1.0928	1.0931
4	12.8908	12.8796	0.8483	0.8483	1.0697	1.0687
5	13.4413	13.4299	0.9511	0.9438	1.0736	1.0755
6	14.0540	14.0516	0.9759	0.9759	1.1130	1.1128
7	14.2415	14.2392	0.9985	0.9985	1.1192	1.1190
8	13.8548	13.8473	0.9695	0.9744	1.0996	1.0971
9	13.9206	13.9159	1.0555	1.0555	1.0739	1.0736
10	13.2582	13.2616	0.9434	0.9434	1.0618	1.0621
11	13.3951	13.4445	1.0216	1.0216	1.0447	1.0485
12	14.0708	14.0655	1.0052	0.9969	1.1034	1.1060
13	14.0540	14.0308	0.9826	0.9826	1.1104	1.1086
14	13.7735	13.7744	0.9575	0.9575	1.0977	1.0977
15	12.6930	12.7095	0.8465	0.8596	1.0540	1.0499
Without VGs	11.1453	–	0.6709	–	1	–

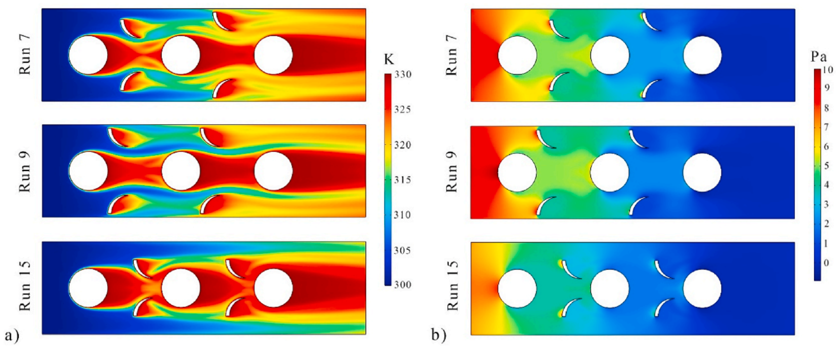

Fig. 6. (a) Contours of temperature and (b) contours of pressure for different FTHE geometry combinations on a plane with a space of 1.5 mm from the fin.

$$\begin{bmatrix} a_1 \\ a_2 \\ a_3 \\ a_4 \end{bmatrix} = \begin{bmatrix} 0.4949 & 0.7854 & 0.1576 \\ -1.6631 & -0.2806 & -0.9376 \\ -1.8722 & -0.2267 & 0.8165 \\ 1.7004 & -1.8830 & 0.3448 \end{bmatrix} \times \begin{bmatrix} 2 \times \dfrac{d_{t1} - 1}{5 - 1} - 1 \\ 2 \times \dfrac{d_{t2} - 1}{5 - 1} - 1 \\ 2 \times \dfrac{d_l - 18}{25 - 18} - 1 \end{bmatrix} + \begin{bmatrix} -1.3000 \\ -0.4712 \\ -0.7409 \\ -0.5437 \end{bmatrix} \tag{25}$$

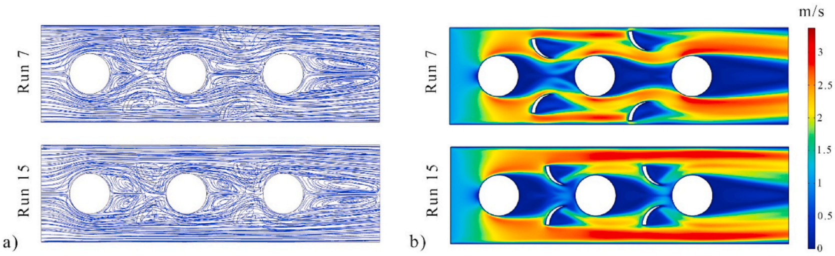

Fig. 7. (a) Streamline and (b) contours of velocity (on a plane with a space of 1.5 mm from the fin) for different FTHE geometry combinations.

Table 8
Nonlinear error functions for fitting measurement.

Error function	Mathematical equation	ANN	
		Nu	ff
R^2	$1-\frac{\sum_{i=1}^{m}(r_{num}-r_{pred})^2}{\sum_{i=1}^{m}(r_{num}-\overline{r_{pred}})^2}$	0.9988	0.9937
RMSE	$\sqrt{\frac{\sum_{i=1}^{m}(r_{pred}-r_{num})^2}{m}}$	0.0156	0.0046
Δq (%)	$100\times\sqrt{\sum_{i=1}^{m}\left(1-\frac{r_{pred}}{r_{num}}\right)^2}$	0.4505	1.9780

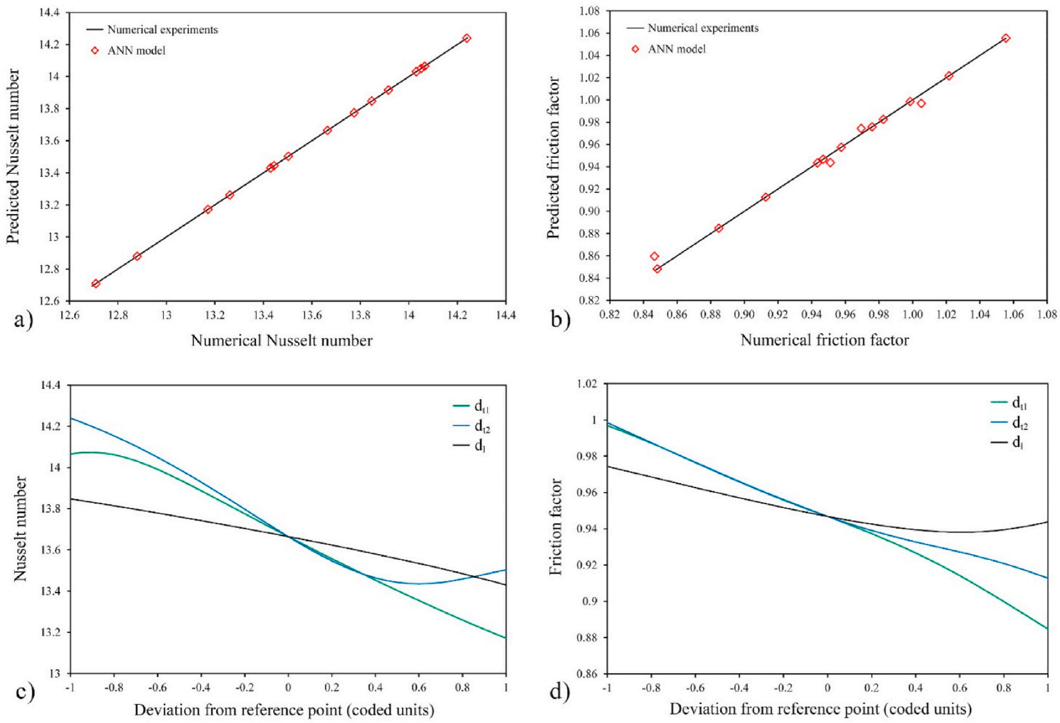

Fig. 8. Comparison of (a) *Nu* and (b) *ff* responses predicted by ANN model and obtained by numerical method, (c) perturbation plot for *Nu* prediction model, (d) perturbation plot for *ff* prediction model.

$$\mathrm{Nu}=\left(\begin{bmatrix}-1.3000 & -0.4712 & -0.7409 & -0.5437\end{bmatrix}\times\begin{bmatrix}\dfrac{2}{1+\exp(-2a_1)}-1\\ \dfrac{2}{1+\exp(-2a_2)}-1\\ \dfrac{2}{1+\exp(-2a_3)}-1\\ \dfrac{2}{1+\exp(-2a_4)}-1\end{bmatrix}+[-0.5426]+1\right)\times\frac{14.2415-12.6930}{2}+12.6930 \tag{26}$$

The model obtained by the artificial neural network method for the *ff* is presented in Eq. (28). The current model incorporates optimized weights and biases, resulting in high predictive accuracy. Based on the R^2 parameter (Table 7), the model demonstrates an impressive prediction capability, accurately predicting 99.37% of the data. Only 0.63% of the *ff* results are not correctly predicted by this model, which indicates the remarkable accuracy of the model in predicting the responses. Also, For the convenience of comparing the results of numerical simulations and prediction models, Fig. 8a and b were presented. As can be seen, there is a negligible discrepancy between the numerical and predicted data due to the high accuracy of the models obtained from the ANN method. Furthermore, no systematic bias was observed in the predictions because there are both over and under-values from the numerical data. Due to the high accuracy of these models in predicting the responses, the effect of selected geometrical factors on the performance of FTHE was investigated using these models, and optimal geometry was presented using the GA method.

$$\begin{bmatrix}b_1\\ b_2\\ b_3\\ b_4\end{bmatrix}=\begin{bmatrix}-0.0775 & 0.7904 & -2.3422\\ -0.4462 & -0.6368 & -0.4926\\ 1.4576 & 0.9890 & -0.5047\\ 2.0870 & -2.3157 & -0.2895\end{bmatrix}\times\begin{bmatrix}2\times\dfrac{d_{t1}-1}{5-1}-1\\ 2\times\dfrac{d_{t2}-1}{5-1}-1\\ 2\times\dfrac{d_l-18}{25-18}-1\end{bmatrix}+\begin{bmatrix}2.4023\\ -0.5674\\ -1.3514\\ 1.2040\end{bmatrix} \tag{27}$$

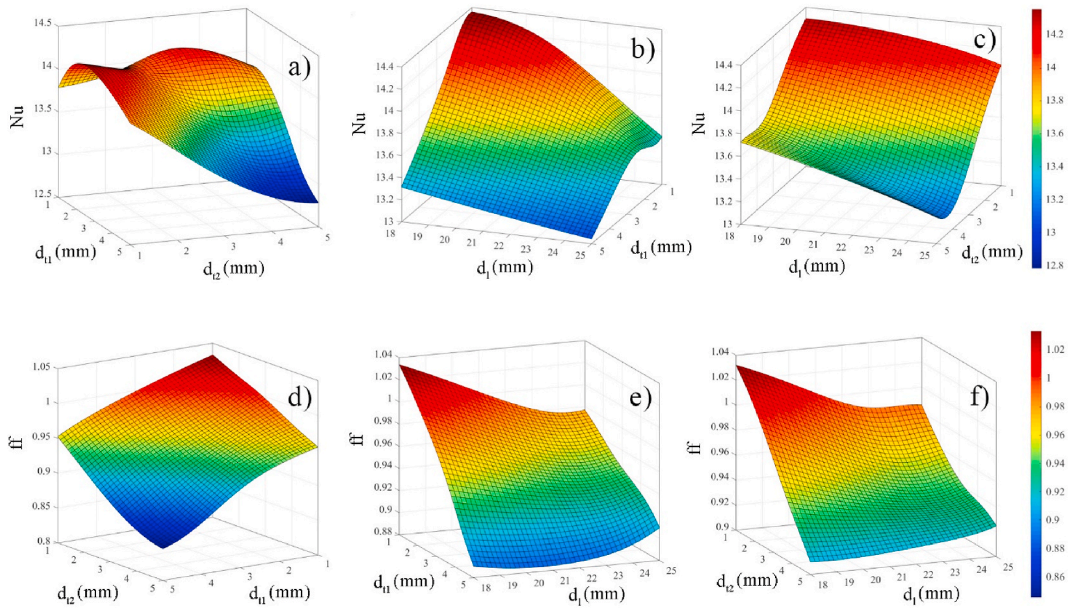

Fig. 9. The three-dimensional diagrams of the effect of input variables on responses.

$$\mathrm{ff}=\left(\left[-0.1573 \quad 0.7849 \quad -0.3889 \quad -0.0814\right]\times\begin{bmatrix}\frac{2}{1+\exp(-2\mathrm{b}_1)}-1\\ \frac{2}{1+\exp(-2\mathrm{b}_2)}-1\\ \frac{2}{1+\exp(-2\mathrm{b}_3)}-1\\ \frac{2}{1+\exp(-2\mathrm{b}_4)}-1\end{bmatrix}+[0.2453]+1\right)\times\frac{1.0555-0.8465}{2}+0.8465 \tag{28}$$

To individually assess the impact of each chosen geometry parameter (d_{t1}, d_{t2}, and d_l) on the model outcomes, Fig. 8c and d was reported. These plots show the effect of the input variables on *Nu* and *ff* of the heat exchanger, and the intensity of this effect can also be seen from these plots. To draw these plots, one of the variables changes in the range of −1 to +1, and the other two remain constant at the 0 levels. As seen in Fig. 8c, generally, *Nu* decreases with the increase of all three geometrical parameters, and d_{t1} and d_l have the greatest and least impact on this response, respectively. Of course, it should be noted that the increase of the d_{t2} parameter after passing a certain level increases *Nu*. According to Fig. 8d, by increasing the parameters from the lowest to the highest level, the heat exchanger's *ff* also decreases, which indicates the improvement of the hydraulic performance. Upon careful examination of the diagram, it becomes evident that the influence of the d_{t1} parameter on the *ff* is remarkably more significant than other parameters. Additionally, due to its minimal slope, the d_l parameter has a low effect on *ff* and hydraulic performance.

In the next step, the effect of two-by-two parameters at different levels on the responses was investigated using three-dimensional diagrams. Fig. 9 presents the analysis of the impact and sensitivity of geometrical variables about the value of *Nu* and *ff*. Fig. 9a shows the effect of changing two geometric variables, d_{t1} and d_{t2}, on *Nu*. This surface plot confirms the results of Fig. 9a that the increase in each parameter of d_{t1} and d_{t2} decreases *Nu*. According to Fig. 9b, the increase of d_l causes a decrease in the value of *Nu*, and this decrease is more intense at the lower d_{t1} parameter; on the other hand, as seen in Fig. 9c, the intensity of the decline of *Nu* with the increase of d_l is greater at higher d_{t2} parameter. From Fig. 9b, it can be concluded that *Nu* decrements with the rise of d_{t1}, and the speed of this decrease is higher at lower d_l. The effect of changes in parameters d_{t1} and d_{t2} on the *ff* of the heat exchanger is shown in Fig. 9d. From this figure, it can be concluded that with the increase of both mentioned geometrical parameters, *ff* decreases significantly. According to Fig. 9e, with the increase in the value of d_{t1}, the response of *ff* decreases remarkably, and this decrease is more severe in lower d_l. Fig. 9f also has a structure similar to Fig. 10e and shows that the effect of two parameters, d_{t1} and d_{t2} on the hydraulic performance of the heat exchanger are close to each other, and in general, with the increase of d_{t2}, *ff* decreases. Also, these figures show that the d_l parameter has an inverse effect on *ff*, so this response decreases with the increase of the d_l geometric parameter. Of course, this statement is not valid at geometries with large d_{t1} and d_{t2}; in these levels, the *ff* increases slightly with d_l increase.

3.3. Results of single-objective and multi-objective optimizations

One of the main goals of this research is to present the optimal placement of vortex generators in FTHE, as shown in Table 9. This optimization was done for three modes: maximum Nusselt number, which only includes thermal performance; minimum friction factor, which is only related to hydraulic performance; and maximum relative efficiency index, which considers both thermal and hydraulic performance of FTHE. As discussed before and presented in this table, the lowest pressure drop and friction factor occur when the VGs are inclined inward and the sides of the path are free for easy flow. Also, the best thermal performance occurs when the VGs can prevent the flow from passing effortlessly, have more contact with the flow, and produce suitable vortices. Table 8 shows that the best performance of FTHE by using the relative efficiency index is obtained in $d_{t1} = 1.3920$ mm, $d_{t2} = 3.8440$ mm, and $d_l = 19.2075$ mm, and this combination of VGs can increase the overall performance of FTHE by 12.78% compared to the case without VG. Finally, the presented geometric model was designed and numerically investigated to check the accuracy of predicting the most optimal state. The value of the relative efficiency index for this heat exchanger was calculated to be 1.1312, and the prediction made has an error of 0.3% compared to the actual results. This geometric design has the highest value of η among the investigated cases, and it can be pointed out that the predicting methods work correctly. Next, FTHE with bow-shaped VGs with the lowest efficiency was predicted. This design has $d_{t1} = 4.1300$ mm, $d_{t2} = 4.5700$ mm, and $d_l = 25$ mm, and the η value for this design was 1.0467. The value of 1.0467 indicates that the efficiency of this heat exchanger has increased by 4.67% compared to the heat exchanger without vortex generators. Arguing from this issue, it can be understood that by adding this type of VGs to FTHE, the total efficiency increases by 4.67% in the worst case. Based on the predicted optimal designs (design with highest η), it becomes evident that for maximizing overall performance, the positioning of vortex generators is crucial in directing the flow inward to foster mixing and generate more vortices. In this design, the first-stage VGs were positioned on the sides, while the second-stage generators were slightly elevated above the first-stage VGs to guide the flow toward the center and promote increased interaction with both the generators and tubes. These processes increase the heat transfer and also increase the pressure drop in the heat exchanger. Fig. 10 shows the contours of FTHE with the optimal design, and according to these contours, the points mentioned above can be better understood. On the contrary, upon examination of the optimal design pertaining to pressure drop (the design characterized by the lowest pressure drop), it is observed that both stages of VGs were positioned near the center and aligned with each other. This arrangement reduces interaction between the fluid and the VGs and tubes, thereby minimizing the formation of vortices. Consequently, the fluid easily passes through the sides and reduces the pressure drop created in the FTHE.

Fig. 11 shows the results of multi-objective optimization investigation. The plot of the Pareto front related to *Nu* and *ff* responses is shown in Fig. 11a. Also, the data associated with the geometric variables of the optimal points of this multi-objective optimization are

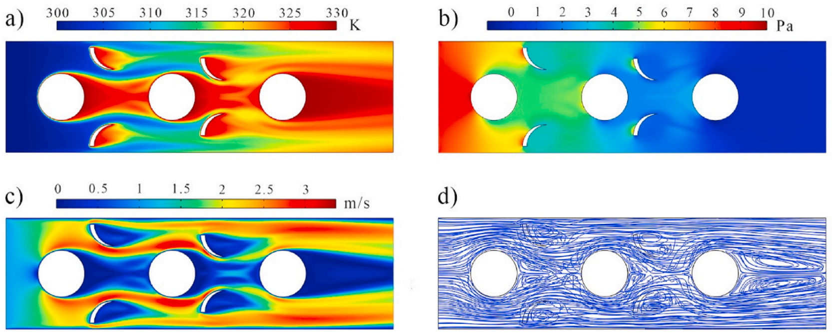

Fig. 10. Optimal design's (a) thermal contour, (b) pressure contour, (c) velocity contour and (d) streamline.

Table 9
Optimizing responses and required design for this performance.

Optimized parameter	Value of inputs			Value of responses		
	d_{t1} (mm)	d_{t2} (mm)	d_l (mm)	*Nu*	ff	η
Nu (maximize)	1.2040	3.4200	18	14.3956	1.0208	1.1230
ff (minimize)	5	5	20.5865	12.8016	0.8449	1.0637
η (maximize)	1.3920	3.8440	19.2075	14.3257	0.9932	1.1278

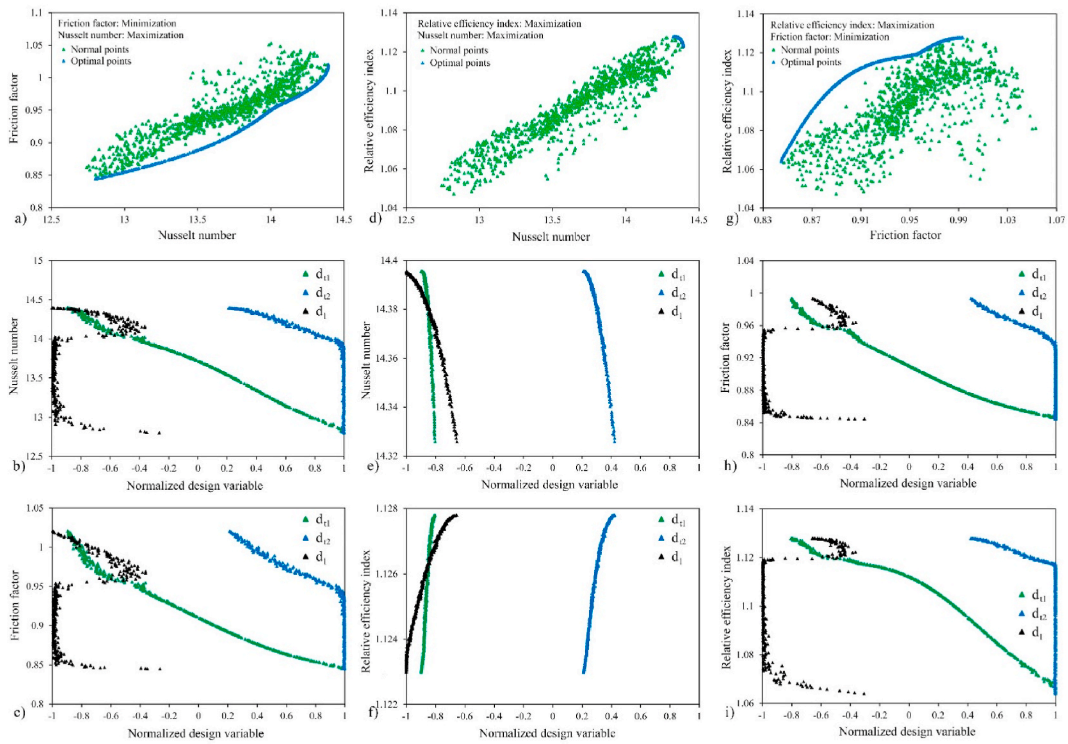

Fig. 11. Multi-objective optimization plots.

presented in Fig. 11b and c. Using these data, it can be concluded that to achieve optimal points with maximum *Nu* and minimum *ff* conditions, the d_{t2} parameter value should be greater than 3.4282 mm, and the d_l parameter value should be smaller than 21.5752 mm. This is while the d_{t1} parameter value is variable and not concentrated in a particular range. The Pareto front for responses of η and *Nu* was shown in Fig. 11d. Plots in Fig. 11e and f shows that in order to reach these optimal points, changes in geometric variables are done in limited areas. This range of changes for the d_{t1} parameter is between 1.2023 mm and 1.3921 mm, for the d_{t2} parameter between 3.4176 mm and 3.8453 mm, and for the d_l parameter between 18.0004 mm and 19.2061 mm. The heat exchanger with the maximum value of Nu and η can be obtained by choosing the geometrical parameters in this range. Fig. 11g also shows the results of the Pareto front for responses η and ff. In this optimization, the response value η was maximized, and ff was minimized. The range of variables related to this optimization is very close to the range of variables associated with the optimization of Fig. 11a.

3.4. Energy balance analysis

In the current section, Table 10 was presented to offer a comprehensive assessment of the optimal heat exchanger's performance and to facilitate a comparison with the FTHE without VGs. The data in this table are based on the results of numerical analysis. As can be seen, the thermal performance of the optimal design at a mass flow rate of 0.1169 g/s is better than the design without VGs, and at the same time, it requires more pumping power (*PP*). To equal the thermal power (*Q*) of the design without VGs with the thermal power of the optimal design, the input mass flow rate of the heat exchanger must be increased to 0.1403 g/s. In this condition, both designs' heat power is almost equal, but as can be seen, the Nusselt number of the optimal design is still higher, which indicates the high heat transfer coefficient of air in this design. Of course, it should be noted that the pumping power required for the FTHE without VGs is higher in this situation (8.5% higher than *PP* of optimal design). In the next step, the input mass flow rate of the heat exchanger without VGs was increased to 0.1791 g/s so that the Nusselt number of this design was equal to the optimal design's Nusselt number. In this condition, the required pumping power of the FTHE without VGs increases by 108.73% compared to the pumping power of the FTHE with optimal design. In comparison, thermal power only experiences an increase of 27%.

In general, there are two main factors to increase the heat transfer in this system, and changing the input flow rate affects these factors in some way. These two factors include heat transfer coefficient (h) and LMTD (expressing the temperature difference between fluid and hot walls), which are related to each other according to Eq. (19). If the temperature difference between the walls and the fluid is high when reaching the desired heat transfer value, it means that the heat transfer coefficient is low. This issue shows that the performance of the device is not suitable, and to compensate for this weakness, the input flow rate has been increased. On the other hand, if the LMTD value is low, it means that the temperature of the heat walls and the fluid have approached each other, and according to this issue and Eq. (18), it can be understood that the flow rate in this state is lower than in the previous state (because the temperature difference between the inlet and outlet of the fluid has increased). Also, in this case, the value of the heat transfer coefficient is high, which indicates the proper performance of the device in the heat transfer process.

It should also be pointed out that there is no limit to increasing the flow rate of the incoming flow. The required pumping power is reasonable and can be easily provided. Of course, it should be noted that this pumping power is required for one unit (distance between two fins) of the heat exchanger, and to get the total pumping power, the number of units must be multiplied by this amount of pumping power. Moreover, due to the low-pressure conditions and the compatibility of the heat exchanger material, there will be no issues concerning device deformation or damage. Under the conditions of these designs, the compressibility of the air is negligible and does not affect the calculation of the flow rate.

4. Conclusions

The main goal of this study is to optimize the thermal-hydraulic performance of an FTHE by adding four bow-shaped VGs on the fins. A hybrid computational approach combining CFD and ANN was employed to achieve this. One of the reasons for using this type of VG is to direct the fluid flow from the outside of the channels to the inside and around the tubes. On the other hand, these VGs can create larger and more vortices behind them. Also, this shape can generate less drag, improving the flow's hydraulic performance compared to other shapes. Three geometric parameters of the VGs (d_{t1}, d_{t2}, and d_l) were considered as input variables, while the parameters Nu and ff served as the research responses. Through changing these geometric parameters, the configuration of VGs on the fins is altered, thus influencing fluid flow dynamics. Based on the numerical analysis results, separate ANNs were trained for each response, and prediction models were developed for each. The findings of this study revealed that.

- The ANN models achieved determination coefficients of 99.88% for Nu and 99.37% for ff, demonstrating high accuracy in predicting the thermal-hydraulic outcomes of the FTHE.
- The increase of all three geometrical variables generally decreases Nu and ff, and the slope of ff changes is much higher.
- In relation to the thermal-hydraulic performance of FTHE, variable d_l has a relatively less impact than other variables.
- According to the definition of the relative efficiency index, the most optimal design of the FTHE was obtained in the geometrical combination of $d_{t1} = 1.920$ mm, $d_{t2} = 3.8440$ mm, and $d_l = 19.2075$ mm, which generally improves the performance by 13.12% compared to the geometry without vortex generators.
- To match the Nu of the FTHE without VGs to that of the optimized design, the inlet flow rate needs a 53.20% increase. However, this amplification in flow rate results in a substantial 108.73% rise in the heat exchanger's pumping power compared to the optimal design.

Table 10
Analyzing the performance disparity between the optimally designed FTHE and FTHE without VGs across diverse operational scenarios.

FTHE design	Re	$\dot{m}$ (g/s)	Nu	Q (W)	PP (mW)
Optimal design	500	0.1169	14.3809	3.0451	0.8472
Without VGs	500	0.1169	11.1453	2.7404	0.5709
	600	0.1403	12.3443	3.0497	0.9191
	766	0.1791	14.3643	3.8740	1.7684

CRediT authorship contribution statement

Zhiqing Bai: Supervision, Methodology. **Azher M. Abed:** Conceptualization, Data curation. **Pradeep Kumar Singh:** Formal analysis, Resources. **Dilsora Abduvalieva:** Investigation, Formal analysis. **Salem Alkhalaf:** Data curation, Writing – review & editing. **Yasser Elmasry:** Project administration, Funding acquisition. **Amani Alruwaili:** Resources, Funding acquisition, Writing – review & editing. **Fawaz S. Alharbi:** Validation, Writing – original draft. **Fahid Riaz:** Writing – original draft, Resources, Formal analysis.

Declaration of competing interest

The authors declare that they have no known competing financial interests or personal relationships that could have appeared to influence the work reported in this paper.

Data availability

The authors do not have permission to share data.

Acknowledgement

The authors extend their appreciation to the Deanship of Scientific Research at King Khalid University for funding this work through the Large Groups under grant number (RGP.2/585/44). The authors extend their appreciation to the Deanship of Scientific Research at Northern Border University, Arar, KSA for funding this research work through the project number "NBU-FPEJ-2024-885-01".

References

[1] A. Elghool, F. Basrawi, T.K. Ibrahim, K. Habib, H. Ibrahim, D.M.N.D. Idris, A review on heat sink for thermo-electric power generation: classifications and parameters affecting performance, Energy Convers. Manag. 134 (2017) 260–277, https://doi.org/10.1016/j.enconman.2016.12.046.

[2] H. Rostamzadeh, M. Feili, H. Ghaebi, Double-flash enhanced Kalina-based binary geothermal power plants, Thermodyn. Anal. Optim. Geotherm. Power Plants (2021) 167–184, https://doi.org/10.1016/B978-0-12-821037-6.00009-3. Elsevier.

[3] J.-Y. Jang, J.-Y. Yang, Experimental and 3-D numerical analysis of the thermal-hydraulic characteristics of elliptic finned-tube heat exchangers, Heat Tran. Eng. 19 (1998) 55–67, https://doi.org/10.1080/01457639808939936.

[4] A. Farajollahi, M. Rostami, M. Feili, H. Ghaebi, Thermodynamic and economic evaluation and optimization of the applicability of integrating an innovative multi-heat recovery with a dual-flash binary geothermal power plant, Clean Technol. Environ. Policy 25 (2023) 1673–1698, https://doi.org/10.1007/s10098-023-02465-8.

[5] H. Wei, H. Moria, K.S. Nisar, R. Ghandour, A. Issakhov, Y.-L. Sun, et al., Effect of volume fraction and size of Al2O3 nanoparticles in thermal, frictional and economic performance of circumferential corrugated helical tube, Case Stud. Therm. Eng. 25 (2021) 100948, https://doi.org/10.1016/j.csite.2021.100948.

[6] Z. Cheng, Z. Guo, P. Fu, J. Yang, Q. Wang, New insights into the effects of methane and oxygen on heat/mass transfer in reactive porous media, Int. Commun. Heat Mass Tran. 129 (2021) 105652, https://doi.org/10.1016/j.icheatmasstransfer.2021.105652.

[7] S. Nekahi, K. Vaferi, S. Nekahi, M. Vajdi, F. Sadegh Moghanlou, N. Baydogan, et al., Finned heat exchangers made of TiB2–SiC–graphene composites with enhanced heat transfer performance, J Brazilian Soc Mech Sci Eng 45 (2023) 497, https://doi.org/10.1007/s40430-023-04362-z.

[8] X. Qi, F. Yu, Z. Meng, Z. Sun, N. Zhang, Z. Guo, Preliminary design of the suppressive containment system based on HPR1000, Nucl. Eng. Des. 415 (2023) 112743, https://doi.org/10.1016/j.nucengdes.2023.112743.

[9] A. Cao, Y. Hua, Z. Sun, Z. Meng, Z. Guo, N. Zhang, Study on reduction of pressure oscillation in low-velocity steam jet condensation, Ann. Nucl. Energy 197 (2024) 110271, https://doi.org/10.1016/j.anucene.2023.110271.

[10] S. Dogan, S. Darici, M. Ozgoren, Numerical comparison of thermal and hydraulic performances for heat exchangers having circular and elliptic cross-section, Int. J. Heat Mass Tran. 145 (2019) 118731, https://doi.org/10.1016/j.ijheatmasstransfer.2019.118731.

[11] M. Feili, M. Hasanzadeh, H. Ghaebi, E. Abdi Aghdam, Comprehensive analysis of a novel cooling/electricity cogeneration system driven by waste heat of a marine diesel engine, Energy Sources, Part A Recover Util Environ Eff 44 (2022) 7331–7346, https://doi.org/10.1080/15567036.2022.2108167.

[12] H. Naik, S. Tiwari, Thermal performance analysis of fin-tube heat exchanger with staggered tube arrangement in presence of rectangular winglet pairs, Int. J. Therm. Sci. 161 (2021) 106723, https://doi.org/10.1016/j.ijthermalsci.2020.106723.

[13] A. Sadeghianjahromi, C.-C. Wang, Heat transfer enhancement in fin-and-tube heat exchangers – a review on different mechanisms, Renew. Sustain. Energy Rev. 137 (2021) 110470, https://doi.org/10.1016/j.rser.2020.110470.

[14] A. Sadeghianjahromi, S. Kheradmand, H. Nemati, C.-C. Wang, Heat transfer enhancement of wavy fin-and-tube heat exchangers via innovative compound designs, Int. J. Therm. Sci. 149 (2020) 106211, https://doi.org/10.1016/j.ijthermalsci.2019.106211.

[15] X. Zhang, Y. Wang, M. Yang, G. Geng, Toward concurrent video multicast orchestration for caching-assisted mobile networks, IEEE Trans. Veh. Technol. 70 (2021) 13205–13220, https://doi.org/10.1109/TVT.2021.3119429.

[16] G. Wang, N. Qian, G. Ding, Heat transfer enhancement in microchannel heat sink with bidirectional rib, Int. J. Heat Mass Tran. 136 (2019) 597–609, https://doi.org/10.1016/j.ijheatmasstransfer.2019.02.018.

[17] A.H. Al-Tohamy, O.G. Fadodun, A. Kaood, Hydrothermal performance of a turbulent nanofluid with different nanoparticle shapes in a duct fitted with various configurations of coiled-wire inserts, J. Therm. Anal. Calorim. 148 (2023) 7795–7810, https://doi.org/10.1007/s10973-023-12241-x.

[18] O.G. Fadodun, A. Kaood, M.A. Hassan, Investigation of the entropy production rate of ferrosoferric oxide/water nanofluid in outward corrugated pipes using a two-phase mixture model, Int. J. Therm. Sci. 178 (2022) 107598, https://doi.org/10.1016/j.ijthermalsci.2022.107598.

[19] M.A. Hassan, M.A. Kassem, A. Kaood, Numerical investigation and multi-criteria optimization of the thermal–hydraulic characteristics of turbulent flow in conical tubes fitted with twisted tape insert, J. Therm. Anal. Calorim. 147 (2022) 6847–6868, https://doi.org/10.1007/s10973-021-10998-7.

[20] K. Vaferi, M. Vajdi, S. Nekahi, S. Nekahi, F. Sadegh Moghanlou, S. Azizi, et al., Numerical simulation of cooling performance in microchannel heat sinks made of AlN ceramics, Microsyst. Technol. 29 (2023) 141–156, https://doi.org/10.1007/s00542-022-05400-x.

[21] Q. Liu, Y. Tao, L. Shi, T. Zhou, Y. Huang, Y. Peng, et al., Parametric optimization of a spiral ground heat exchanger by response surface methodology and multi-objective genetic algorithm, Appl. Therm. Eng. 221 (2023) 119824, https://doi.org/10.1016/j.applthermaleng.2022.119824.

[22] X. Bai, Y. He, M. Xu, Low-thrust reconfiguration strategy and optimization for formation flying using Jordan normal form, IEEE Trans. Aero. Electron. Syst. 57 (2021) 3279–3295, https://doi.org/10.1109/TAES.2021.3074204.

[23] S. Yang, Z. Huang, Q. Hu, Y. Zhang, F. Wang, H. Wang, et al., Proportional optimization model of multiscale spherical BN for enhancing thermal conductivity, ACS Appl. Electron. Mater. 4 (2022) 4659–4667, https://doi.org/10.1021/acsaelm.2c00878.

[24] L.-C. Jia, Z.-X. Wang, L. Wang, J.-F. Zeng, P.-Y. Du, Y.-F. Yue, et al., Self-standing boron nitride bulks enabled by liquid metals for thermal management, Mater. Horiz. 10 (2023) 5656–5665, https://doi.org/10.1039/D3MH01359F.

[25] M. Awais, A.A. Bhuiyan, Heat transfer enhancement using different types of vortex generators (VGs): a review on experimental and numerical activities, Therm. Sci. Eng. Prog. 5 (2018) 524–545, https://doi.org/10.1016/j.tsep.2018.02.007.
[26] M. Veerabhadrappa Bidari, P.B. Nagaraj, G. Lalagi, Influence of different types of vortex generators (VGs) to enhance heat transfer performance in heat exchangers: a review, Int. J. Ambient Energy 43 (2022) 5718–5741, https://doi.org/10.1080/01430750.2021.1980740.
[27] M. Dogan, S. Erzincan, Experimental investigation of thermal performance of novel type vortex generator in rectangular channel, Int. Commun. Heat Mass Tran. 144 (2023) 106785, https://doi.org/10.1016/j.icheatmasstransfer.2023.106785.
[28] A. Sadeghianjahromi, S. Kheradmand, H. Nemati, J.-S. Liaw, C.-C. Wang, Compound heat transfer enhancement of wavy fin-and-tube heat exchangers through boundary layer restarting and swirled flow, Energies 11 (2018) 1959, https://doi.org/10.3390/en11081959.
[29] M. Fiebig, P. Kallweit, N. Mitra, S. Tiggelbeck, Heat transfer enhancement and drag by longitudinal vortex generators in channel flow, Exp. Therm. Fluid Sci. 4 (1991) 103–114, https://doi.org/10.1016/0894-1777(91)90024-L.
[30] P. Wang, J. Jiang, S. Li, X. Luo, S. Wang, W. Zhao, An investigation of influence factor including different tube bundles on inclined elliptical fin-tube heat exchanger, Int. J. Heat Mass Tran. 142 (2019) 118448, https://doi.org/10.1016/j.ijheatmasstransfer.2019.118448.
[31] R. kumar, R. Kumar, S. Kumar, S. Thapa, M. Sethi, G. Fekete, et al., Impact of artificial roughness variation on heat transfer and friction characteristics of solar air heating system, Alex. Eng. J. 61 (2022) 481–491, https://doi.org/10.1016/j.aej.2021.06.031.
[32] B. Lotfi, B. Sundén, Q. Wang, An investigation of the thermo-hydraulic performance of the smooth wavy fin-and-elliptical tube heat exchangers utilizing new type vortex generators, Appl. Energy 162 (2016) 1282–1302, https://doi.org/10.1016/j.apenergy.2015.07.065.
[33] L.-T. Tian, Y.-L. He, Y.-G. Lei, W.-Q. Tao, Numerical study of fluid flow and heat transfer in a flat-plate channel with longitudinal vortex generators by applying field synergy principle analysis, Int. Commun. Heat Mass Tran. 36 (2009) 111–120, https://doi.org/10.1016/j.icheatmasstransfer.2008.10.018.
[34] A. Kaood, A. Aboulmagd, H. Othman, A. ElDegwy, Numerical investigation of the thermal-hydraulic characteristics of turbulent flow in conical tubes with dimples, Case Stud. Therm. Eng. 36 (2022) 102166, https://doi.org/10.1016/j.csite.2022.102166.
[35] H.Z. Demirağ, M. Doğan, A.A. İğci, The experimental and numerical investigation of novel type conic vortex generator on heat transfer enhancement, Int. J. Therm. Sci. 191 (2023) 108383, https://doi.org/10.1016/j.ijthermalsci.2023.108383.
[36] K. Torii, K.M. Kwak, K. Nishino, Heat transfer enhancement accompanying pressure-loss reduction with winglet-type vortex generators for fin-tube heat exchangers, Int. J. Heat Mass Tran. 45 (2002) 3795–3801, https://doi.org/10.1016/S0017-9310(02)00080-7.
[37] A. Kaood, O.G. Fadodun, Numerical investigation of turbulent entropy production rate in conical tubes fitted with a twisted-tape insert, Int. Commun. Heat Mass Tran. 139 (2022) 106520, https://doi.org/10.1016/j.icheatmasstransfer.2022.106520.
[38] M. Mohanraj, S. Jayaraj, C. Muraleedharan, Applications of artificial neural networks for thermal analysis of heat exchangers – a review, Int. J. Therm. Sci. 90 (2015) 150–172, https://doi.org/10.1016/j.ijthermalsci.2014.11.030.
[39] D. Chen, Q. Wang, Y. Li, Y. Li, H. Zhou, Y. Fan, A general linear free energy relationship for predicting partition coefficients of neutral organic compounds, Chemosphere 247 (2020) 125869, https://doi.org/10.1016/j.chemosphere.2020.125869.
[40] O. Duran, N. Rodriguez, L.A. Consalter, Neural networks for cost estimation of shell and tube heat exchangers, Expert Syst. Appl. 36 (2009) 7435–7440, https://doi.org/10.1016/j.eswa.2008.09.014.
[41] A. Lambora, K. Gupta, K. Chopra, Genetic algorithm- A literature review, in: 2019 Int. Conf. Mach. Learn. Big Data, Cloud Parallel Comput., IEEE, 2019, pp. 380–384, https://doi.org/10.1109/COMITCon.2019.8862255.
[42] F. Li, T.C.A. Kumar, Y. Elmasry, P.K. Singh, A.M. Abed, A.D. Algarni, et al., Response Surface Methodology and Artificial Neural Network modellings on hydraulic and thermal performances of a disk-shaped heat sink with tree-like microchannels, Case Stud. Therm. Eng. 40 (2022) 102539, https://doi.org/10.1016/j.csite.2022.102539.
[43] M.H. Mohammadi, H.R. Abbasi, A. Yavarinasab, H. Pourrahmani, Thermal optimization of shell and tube heat exchanger using porous baffles, Appl. Therm. Eng. 170 (2020) 115005, https://doi.org/10.1016/j.applthermaleng.2020.115005.
[44] R. Aghayari, H. Maddah, S.M. Pourkiaei, M.H. Ahmadi, L. Chen, M. Ghazvini, Theoretical and experimental studies of heat transfer in a double-pipe heat exchanger equipped with twisted tape and nanofluid, Eur Phys J Plus 135 (2020) 252, https://doi.org/10.1140/epjp/s13360-020-00252-8.
[45] K. Sharifi, M. Sabeti, M. Rafiei, A.H. Mohammadi, A. Ghaffari, M.H. Asl, et al., A good contribution of computational fluid dynamics (CFD) and GA-ANN methods to find the best type of helical wire inserted tube in heat exchangers, Int. J. Therm. Sci. 154 (2020) 106398, https://doi.org/10.1016/j.ijthermalsci.2020.106398.
[46] S. Chamoli, ANN and RSM approach for modeling and optimization of designing parameters for a V down perforated baffle roughened rectangular channel, Alex. Eng. J. 54 (2015) 429–446, https://doi.org/10.1016/j.aej.2015.03.018.
[47] C. Xie, G. Yan, Q. Ma, Y. Elmasry, P.K. Singh, A.M. Algelany, et al., Flow and heat transfer optimization of a fin-tube heat exchanger with vortex generators using Response Surface Methodology and Artificial Neural Network, Case Stud. Therm. Eng. 39 (2022) 102445, https://doi.org/10.1016/j.csite.2022.102445.
[48] G. Xie, B. Sunden, Q. Wang, L. Tang, Performance predictions of laminar and turbulent heat transfer and fluid flow of heat exchangers having large tube-diameter and large tube-row by artificial neural networks, Int. J. Heat Mass Tran. 52 (2009) 2484–2497, https://doi.org/10.1016/j.ijheatmasstransfer.2008.10.036.
[49] A. Sinha, H. Chattopadhyay, A.K. Iyengar, G. Biswas, Enhancement of heat transfer in a fin-tube heat exchanger using rectangular winglet type vortex generators, Int. J. Heat Mass Tran. 101 (2016) 667–681, https://doi.org/10.1016/j.ijheatmasstransfer.2016.05.032.
[50] J. Fontchastagner, T. Lubin, S. Mezani, N. Takorabet, Design optimization of an axial-field eddy-current magnetic coupling based on magneto-thermal analytical model, Open Phys. 16 (2018) 21–26, https://doi.org/10.1515/phys-2018-0004.
[51] D.C. Wilcox, Turbulence Modeling for CFD, first ed., DCW Industries, Inc., La Canada, CA, USA, 1998, pp. 73–170, n.d.
[52] G.D. Di Martino, C. Carmicino, S. Mungiguerra, R. Savino, The application of computational thermo-fluid-dynamics to the simulation of hybrid rocket internal ballistics with classical or liquefying fuels: a review, Aerospace 6 (2019) 56, https://doi.org/10.3390/aerospace6050056.
[53] S.M. Mousavı, N. Shafıeı, A. Dadvand, Numerical simulation of sunsonic turbulent flow over NACA0012 airfoil: evaluation of turbulence models, Sigma J. Eng. Nat. Sci. 35 (1) (2017) 133–155, n.d.
[54] M.E. Nakhchi, J.A. Esfahani, Numerical investigation of different geometrical parameters of perforated conical rings on flow structure and heat transfer in heat exchangers, Appl. Therm. Eng. 156 (2019) 494–505, https://doi.org/10.1016/j.applthermaleng.2019.04.067.
[55] P. Promvonge, S. Skullong, Heat transfer augmentation in solar receiver heat exchanger with hole-punched wings, Appl. Therm. Eng. 155 (2019) 59–69, https://doi.org/10.1016/j.applthermaleng.2019.03.132.
[56] K. Xu, B. Ruan, H. Meng, A thermal performance factor for evaluation of active engine cooling with asymmetric heating, Appl. Therm. Eng. 73 (2014) 351–356, https://doi.org/10.1016/j.applthermaleng.2014.07.066.
[57] C.-C. Wang, Y.-J. Chang, Y.-C. Hsieh, Y.-T. Lin, Sensible heat and friction characteristics of plate fin-and-tube heat exchangers having plane fins, Int. J. Refrig. 19 (1996) 223–230, https://doi.org/10.1016/0140-7007(96)00021-7.
[58] K. Vaferi, M. Vajdi, A. Shadian, H. Ahadnejad, F.S. Moghanlou, H. Nami, et al., Modeling and optimization of hydraulic and thermal performance of a tesla valve using a numerical method and artificial neural network, Entropy 25 (2023) 967, https://doi.org/10.3390/e25070967.
[59] W.S. McCulloch, W. Pitts, A logical calculus of the ideas immanent in nervous activity, Bull. Math. Biophys. 5 (1943) 115–133, https://doi.org/10.1007/BF02478259.
[60] K. Vaferi, M. Vajdi, S. Nekahi, A. Heydari, F. Sadegh Moghanlou, H. Nami, et al., Thermo-hydraulic performance optimization of a disk-shaped microchannel heat sink applying computational fluid dynamics, artificial neural network, and response surface methodology, Heliyon 9 (2023) e21031, https://doi.org/10.1016/j.heliyon.2023.e21031.

[61] M. Shoaib, M.A.Z. Raja, I. Farhat, Z. Shah, P. Kumam, S. Islam, Soft computing paradigm for Ferrofluid by exponentially stretched surface in the presence of magnetic dipole and heat transfer, Alex. Eng. J. 61 (2022) 1607–1623, https://doi.org/10.1016/j.aej.2021.06.060.
[62] H. Ke, T.A. Khan, W. Li, Y. Lin, Z. Ke, H. Zhu, et al., Thermal-hydraulic performance and optimization of attack angle of delta winglets in plain and wavy finned-tube heat exchangers, Appl. Therm. Eng. 150 (2019) 1054–1065, https://doi.org/10.1016/j.applthermaleng.2019.01.083.
[63] X. Liang, N.B. Kumar, I.B. Mansir, P. Kumar Singh, A.M. Abed, M. Dahari, et al., Management of heat transfer and hydraulic characteristics of a micro-channel heat sink with various arrangements of rectangular vortex generators utilizing artificial neural network and response surface methodology, Case Stud. Therm. Eng. 44 (2023) 102850, https://doi.org/10.1016/j.csite.2023.102850.